

An ab initio path integral Monte Carlo simulation method for molecules and clusters: application to Li_4 and Li_5^+

Ruben O. Weht^{a,b}, Jorge Kohanoff^{a*}, Darío A. Estrin^{a,c}, and Charusita Chakravarty^{a,d}

^a *International Centre for Theoretical Physics,
Strada Costiera 11, I-34014 Trieste, Italy*

^b *Comisión Nacional de Energía Atómica,
Avenida Libertador 8250, 1429, Buenos Aires, Argentina*

^c *Departamento de Química Inorgánica, Analítica y Química-Física e INQUIMAE,
Facultad de Ciencias Exactas y Naturales, Universidad de Buenos Aires
Ciudad Universitaria, Pabellón II, 1428, Buenos Aires, Argentina*

^d *Department of Chemistry, Indian Institute of Technology - Delhi
Hauz Khas, New Delhi 110016, India*

(September 11, 2018)

A novel method for simulating the statistical mechanics of molecular systems in which both nuclear and electronic degrees of freedom are treated quantum mechanically is presented. The scheme combines a path integral description of the nuclear variables with a first-principles adiabatic description of the electronic structure. The electronic problem is solved for the ground state within a density functional approach, with the electronic orbitals expanded in a localized (Gaussian) basis set. The discretized path integral is computed by a Metropolis Monte Carlo sampling technique on the normal modes of the isomorphic ring-polymer. An effective short-time action correct to order τ^4 is used. The validity and performance of the method are tested by studying two small Lithium clusters, namely Li_4 and Li_5^+ . Structural and electronic properties computed within this fully quantum-mechanical scheme are presented and compared to those obtained within the classical nuclei approximation. Quantum delocalization effects turn out to be significant as shown by the fact that quantum simulation results at 50 K approximately correspond to those of classical simulations carried out at 150 K. The scaling factor depends, however, on the specific physical property, thus evidencing the different character of quantum and thermal correlations. Tunneling turns out to be irrelevant in the temperature range investigated (50 K to 200 K).

I. INTRODUCTION

Light atoms, such as H, He, Li or Be, cannot very often be treated as classical particles, particularly at low temperatures. As temperature decreases and the thermal de Broglie wavelength increases, the quantum character emerges, and a description in terms of classical coordinates and momenta breaks down. The most obvious manifestation of the quantum character of light atoms is a large zero-point-energy (ZPE). A particle of mass m in a harmonic potential with characteristic frequency ω will have a ZPE of $\hbar\omega/2$ and an associated spatial delocalization of $\Delta x = \sqrt{\hbar/m\omega}$. For instance, a proton in a typical bonding environment such as a H-O bond or a H_2 molecule, will have a ZPE of 0.15 to 0.25 eV and Δx between 0.2 and 0.3 rÅ. This represents a sizeable effect which could be decisive in stabilizing a particular crystalline structure for a solid, or the ground state configuration of a molecule or a cluster. An even more interesting manifestation of quantum effects is the possibility that these light nuclei can tunnel across potential energy barriers, thus exploring classically forbidden regions of configuration space and giving rise to a variety of interesting quantum effects such as temperature-independent diffusion, exotic ground states, resonances in ion-surface

scattering, and fluxional molecules. Signatures of quantum effects can also be observed in low-energy atomic collisions, or in proton-transfer reactions in the gas and condensed phases.

To date, most studies that consider the quantum character of atomic nuclei are based on an empirical description of the interatomic interactions, or otherwise consist of extending and/or correcting *a posteriori* the results obtained within a classical nuclei approximation. Classical potentials are frequently not transferable from one environment to another, and are ill-suited to modeling phenomena involving significant electronic density redistribution, as in the making and breaking of chemical bonds. The natural route to overcome these limitations is to describe the interactions at a first-principles level, i.e. by including explicitly the electronic component in the description of the system. The recent development of such schemes, which address the question of the interplay between electronic structure and the quantum nature of light nuclei, has only very recently begun to be realized, thus opening a fascinating field with important implications in many branches of physics, chemistry and biology.

Since small clusters usually exhibit rich landscapes of isomeric forms within narrow energy bands¹, they constitute good systems for studying the effects of quantum de-

localization and associated tunneling behavior. Lithium clusters are particularly interesting because in addition to the small atomic mass, they are bound by metallic many-body interactions which cannot be adequately represented by means of classical interatomic potentials².

In the remainder of this Introduction we outline the methodology that we have developed to study this class of problems, and review the present understanding of Li clusters which is the test system for our method. In Section II we introduce the theoretical framework of our *ab initio* path integral approach and discuss the approximations involved. Section III is devoted to the details of the practical implementation of the path integral Monte Carlo (PIMC) and the electronic structure methods. In Section IV we present the validation of the electronic structure calculations, zero-temperature geometries and electronic properties of Li_4 and Li_5^+ clusters. The results of our simulations for the classical and quantum Li_4 and Li_5^+ clusters at finite temperatures are presented in Section V. Section VI contains our conclusions and an assessment of the potential of this novel simulation tool.

A. Methodological aspects

The goal of the present work is to introduce a novel computational technique for studying the statistical mechanics of isolated systems like clusters and molecules containing light atoms. Our approach combines an imaginary-time path integral description of the nuclear degrees of freedom³ with a first-principles density functional (DFT) description of the electronic structure⁴. Since the natural choice for investigating isolated systems is to use a localized basis set for the electronic orbitals, we adopt a Gaussian basis set⁵. In the present implementation the electronic structure is computed at the all-electron level, i.e. explicitly including core electrons. The sampling of the path integral is implemented using Monte Carlo (MC) techniques. The electronic energy is minimized for each nuclear configuration, and the MC rejection step is also performed using the energy calculated at the same level of sophistication.

Other schemes along these lines have been recently proposed by Marx and Parrinello⁶, and Cheng et al.⁷. At variance with our approach, these two methods use Molecular Dynamics (MD) for sampling the path integral, a plane-wave (PW) expansion for the electronic orbitals and treat the electron-ion interaction at the pseudopotential level. PW expansions with periodic boundary conditions are more appropriate for extended systems such as solids or liquids though they can be adequately modified to deal with isolated systems⁶.

The evaluation of real-time path integrals, which would include the full dynamical information, is an extremely difficult numerical task because the integrand is a rapid oscillatory function of the path. In the imaginary-time framework the statistical weight is real and positive def-

inite, so that the integrals are well-conditioned, but the price is that the dynamics is not directly accessible. In the absence of real-time dynamical information, it is not particularly advantageous to sample the integral using MD in place of MC techniques. In particular, the MD technique requires elaborate thermostating mechanisms⁸ in order to overcome ergodicity problems in the sampling of the quasi-harmonic degrees of freedom that appear in the path integral formulation (see Section II). In the present method we propose a Metropolis MC sampling technique on the normal modes of the polymer, which has less severe ergodicity problems, and is more convenient from the point of view of efficient evaluation of the path action (see Section III)⁹. Moreover, the MC strategy is easy to interface with any electronic structure code.

B. Small Lithium clusters

Structural and electronic properties of Li_n and Li_n^+ clusters have been systematically investigated for $n = 2 - 9$ by means of *ab initio* configuration-interaction calculations¹⁰. A key observation was the existence of several isomers of comparable energy. Recently, *ab initio* classical MD simulations at the Hartree-Fock (HF) and non-local density functional (NLDF) level were carried out in order to explore the cluster dynamics as a function of temperature, to analyze isomerization reactions, and to study the melting transition¹¹⁻¹⁴. The extent to which different levels of first-principles calculations are reliable for describing small Li clusters has been very recently discussed by Rousseau and Marx¹⁵, who concluded that either *ab initio* MP2 calculations, or gradient corrected NLDF provide a reasonable potential energy landscape, while HF and LDF are inadequate.

This aspect is very important because the energy landscape determines the probability with which the cluster visits different possible geometries. In general, the ability to jump from one minimum to another will depend on the extent of both thermal and quantum fluctuations. Fig. 1 shows three typical situations: At low temperatures quantum delocalization is the dominant mechanism. If the ZPE is higher than the barrier between the two minima (a), or smaller than the barrier but larger than the energy difference between them (b) (tunneling regime), the ground state wave function will sample both configurational minima. If, instead, it is smaller than the energy difference between the two minima (c), then the ground state will be basically unchanged from the classical one, though all structural distributions will be broadened by quantum delocalization. Thermal excitations can promote a classical-like situation like (c) to a thermally-assisted tunneling regime.

The above picture is valid as long as the electronic ground state is non-degenerate, and this is realized for clusters with closed electronic shells. Open-shell clus-

ters undergo Jahn-Teller distortions, and are characterized by degenerate ground states and *pseudo-rotations*. An adequate treatment of this situation would require the introduction of the concepts of conical intersections and geometric phases¹⁶. Though these phenomena are of great interest, and have indeed been detected in Li₃¹⁷ and Li₅¹⁸, we have preferred to avoid this extra complication at this stage in the development of our method.

Quantum nuclear effects in Li clusters were first addressed by Ballone and Milani¹⁹, who studied magic-number clusters (20, 40 and 92 atoms) by means of PIMC simulations using a simple, jellium model description of the electronic component. Their most interesting observation was the existence of a large number of isomers differing only in the location of the outermost atoms, such that quantum tunneling amongst these isomers led to a fluid-like behavior. A very recent ab initio path integral MD study of Li₈ and Li₂₀ clusters by Rousseau and Marx²⁰ shows that this picture does not hold when the description of the electronic component is improved, thus demonstrating the necessity of going beyond the jellium-type description.

For our study we have chosen the following two examples: Li₄ has a single isomer and is well described by a quasi-classical picture. Li₅⁺, has two isomers at an energy difference of about 150 *K*, and two other isomers at higher energies (see section 5). The zero-point-energy is of the order of 100 *K*, so that Li₅⁺ could constitute a good candidate for exhibiting significant quantum effects in terms of the sampling of configurational minima. The results presented in section 5 will show that, in spite of this, Li₅⁺ actually behaves in a very similar way to Li₄.

II. THE AB INITIO PATH INTEGRAL PARTITION FUNCTION

The statistical mechanics of quantum many-body systems can be formulated in terms of the two-point density matrix, or imaginary-time propagator:

$$\rho(\mathbf{R}, \mathbf{R}', \beta) = \langle \mathbf{R} | \exp(-\beta \hat{\mathcal{H}}) | \mathbf{R}' \rangle, \quad (1)$$

whose trace is the partition function \mathcal{Z} . $\beta = 1/k_B T$ is the inverse temperature. The path integral representation of the density matrix is given by

$$\rho(\mathbf{R}, \mathbf{R}', \beta) = \int \mathcal{D}[\mathbf{R}(u)] e^{-S[\mathbf{R}(u)]}, \quad (2)$$

where $\mathbf{R}(u)$ represents the configuration of an N -body system as a function of imaginary time u . The range of u is from 0 to $\beta\hbar$ and the paths considered are restricted to those beginning at $\mathbf{R}(0) = \mathbf{R}$ and ending at $\mathbf{R}(\beta\hbar) = \mathbf{R}'$. The partition function can be similarly expressed as a path integral with contributions from all possible cyclic paths for which $\mathbf{R}(0) = \mathbf{R}(\beta\hbar)$. $\mathcal{D}[\mathbf{R}(u)]$ represents the differential element for all paths. The Euclidean action, $S[\mathbf{R}(u)]$, associated with a path is defined as

$$S[\mathbf{R}(u)] = \frac{1}{\hbar} \int_0^{\beta\hbar} \left(\frac{m}{2} \left[\frac{d\mathbf{R}}{du} \right]^2 + V[\mathbf{R}(u)] \right) du. \quad (3)$$

The first term corresponds to the kinetic energy contribution to the action, with m the mass of the particles. The generalization to heterogeneous systems, i.e. composed of two or more species of different masses, is straightforward.

In order to devise a feasible computational scheme, the path integral is typically discretized by representing the cyclic paths as a finite set of $3N$ -dimensional configurations, \mathbf{R}_i , at equispaced points in imaginary time between 0 and $\beta\hbar$. The degree of discretisation is referred to as the Trotter number, P . The short-time or high temperature propagator, $\rho(\mathbf{R}_i, \mathbf{R}_{i+1}; \beta/P)$, can be evaluated semi-classically at different levels of approximation. The contribution of the kinetic energy term to the short-time action is written in terms of a first-order finite difference between configurations on adjacent time slices, while the short-time integral of the potential energy together with higher-order corrections to the kinetic energy, is replaced with an effective, quantum-corrected potential $V_{eff}(\mathbf{R})$. The sum of the two terms is referred to as the *effective action*. Therefore, the expression for the partition function of N interacting, distinguishable quantum particles with Trotter number P is given by:

$$\mathcal{Z}_{NP} = \left(\frac{mP}{2\pi\hbar^2\beta} \right)^{3NP/2} \int \left(\prod_{i=1}^P d\mathbf{R}_i \right) \times \exp \left(-\frac{mP}{2\hbar^2\beta} \sum_{i=1}^P (\mathbf{R}_i - \mathbf{R}_{i+1})^2 - \frac{\beta}{P} \sum_{i=1}^P V_{eff}(\mathbf{R}_i) \right). \quad (4)$$

According to the level of approximation of the effective action, the number of slices P needed to achieve convergence in the partition function can be small enough that the problem is tractable, or large enough that the evaluation of the multidimensional integral becomes a hopeless task. It is therefore important to use the best possible effective action compatible with the computational complexity involved in its calculation. The simplest one, or *primitive approximation*, replaces the effective potential by the bare potential, which is equivalent to an end-point approximation for the short-time integral:

$$\frac{1}{\hbar} \int_0^{\tau\hbar} V[\mathbf{R}(u)] du \approx \tau \left[\frac{V(\mathbf{R}) + V(\mathbf{R}')}{2} \right], \quad (5)$$

and is correct only to order τ^2 . At the other extreme, the pair-action approximation provides a very accurate technique when the full, many-body potential can be reasonably approximated with a sum of pair potentials. This scheme has been very effectively exploited to investigate the properties of liquid and superfluid He down to temperatures of about 1 *K*²¹, a task that would not have been possible using the primitive action.

As mentioned in the introduction, classical interaction potentials are computationally fast, but very often unreliable. Realistic interaction potentials can instead be

obtained from more expensive first-principles techniques. In these latter, the electronic degrees of freedom are explicitly included in the Hamiltonian description of the system:

$$\hat{\mathcal{H}}(\mathbf{R}, \mathbf{r}) = \hat{T}_n + \hat{T}_e + \hat{V}_{ee}(\mathbf{r}) + \hat{V}_{en}(\mathbf{r}, \mathbf{R}) + \hat{V}_{nn}(\mathbf{R}), \quad (6)$$

where \mathbf{r} and \mathbf{R} are the electronic and nuclear coordinates, \hat{T} and \hat{V} stand for kinetic and potential operators, while subscripts **e** and **n** indicate electronic and nuclear components, respectively. The path integral representation for the partition function could then be developed using the coordinate basis for both the electrons and the nuclei²².

However, standard electronic structure calculations are carried out in a wave function representation by resorting to the adiabatic separation of nuclear and electronic motion. It is therefore more convenient to expand the electronic component in the adiabatic basis set where electronic wave functions $|\phi_\alpha\rangle$ and total energies $E_\alpha(\mathbf{R})$ are obtained by diagonalising the electronic Hamiltonian $\hat{T}_e + \hat{V}_{ee}(\mathbf{r}) + \hat{V}_{en}(\mathbf{r}, \mathbf{R}) + \hat{V}_{nn}(\mathbf{R})$. If $\tau = \beta/P$, then the discretized partition function reads:

$$\mathcal{Z}_P = \sum_{\alpha_1} \cdots \sum_{\alpha_P} \int \cdots \int \prod_{i=1}^P \left(\rho_{\alpha_i, \alpha_{i+1}}(\mathbf{R}_i, \mathbf{R}_{i+1}, \tau) d\mathbf{R}_i \right) \quad (7)$$

where

$$\rho_{\alpha, \gamma}(\mathbf{R}, \mathbf{R}', \tau) = \langle \mathbf{R} | \langle \phi_\alpha | \exp(-\tau \hat{\mathcal{H}}) | \phi_\gamma \rangle | \mathbf{R}' \rangle. \quad (8)$$

Then, in the spirit of expression (4), the short-time propagator can be written as:

$$\rho_{\alpha, \gamma}(\mathbf{R}, \mathbf{R}', \tau) = \langle \mathbf{R} | \langle \phi_\alpha | \exp(-\tau \hat{T}_n) | \phi_\gamma \rangle | \mathbf{R}' \rangle \times \exp\left(-\frac{\tau}{2} [E_\alpha^{eff}(\mathbf{R}) + E_\gamma^{eff}(\mathbf{R}')] \right), \quad (9)$$

where $E_\alpha^{eff}(\mathbf{R})$ is an effective potential which derives directly from the electronic structure. In the primitive approximation, which is what has been used in other *ab initio* path integral methods^{6,7}, the effective potential is simply the total energy corresponding to adiabatic state α of the electronic Hamiltonian, i.e. $E_\alpha(\mathbf{R})$.

The nuclear kinetic energy operator can give rise to non-adiabatic coupling matrix elements between adiabatic eigenstates. If these are negligible, but more than one Born-Oppenheimer (BO) surface is occupied due to thermal excitations, then the partition function will split into independent manifolds indexed by the BO electronic eigenstate. In the absence of degeneracies in the ground electronic state, the energy differences between electronic eigenstates are typically orders of magnitude larger than reasonable thermal kinetic energies. Consequently only the ground electronic state contributes to the partition function and the electrons only enter at the level of replacing the total potential energy with the ground state

first-principles effective potential $E_0^{eff}(\mathbf{R})$ in equation (4):

$$\mathcal{Z}_{NP} = \left(\frac{mP}{2\pi\hbar^2\beta} \right)^{3NP/2} \int \left(\prod_{i=1}^P d\mathbf{R}_i \right) \times \exp\left(-\frac{mP}{2\hbar^2\beta} \sum_{i=1}^P (\mathbf{R}_i - \mathbf{R}_{i+1})^2 - \frac{\beta}{P} \sum_{i=1}^P E_0^{eff}(\mathbf{R}_i) \right). \quad (10)$$

This is the partition function that will be evaluated using Monte Carlo techniques. The expression for \mathcal{Z}_{NP} can be interpreted as the partition function of N classical polymers, each of P monomeric units or beads, with adjacent beads linked by harmonic springs with force constant $mP/\beta\hbar^2$. Beads on two separate cyclic polymers are coupled by the interaction potential only if they lie on the same time slice.

Let us remark that the computation of excited electronic states is an open issue in density functional theory, and it is known that the usual approximations to exchange and correlation, like the LDA and even NLDF do not provide reliable excitation energies. Excited states could be calculated properly using very high-level *ab initio* methods. However, since we have developed a methodology in which the electronic degrees of freedom are dealt within DFT, we are for the time being not in a position to incorporate non-adiabatic couplings and excited electronic manifolds.

III. PRACTICAL IMPLEMENTATION

A. Path integral Monte Carlo

1. Effective action

We use a discretized time representation in which a path is described as a set of configurations, $\{\mathbf{R}_i\}$, $i = 1, \dots, P$, at P -equispaced points in imaginary time. The effective short-time propagator for two adjacent points along the path has been evaluated to fourth-order accuracy in $\tau = \beta/P$, so that the first-principles effective potential reads²³:

$$E_0^{eff}(\mathbf{R}_i) = E_0(\mathbf{R}_i) + \left(\frac{\beta^2\hbar^2}{24mP^2} \right) \sum_{j=1}^N \left(\frac{\partial E_0(\mathbf{R}_i)}{\partial \mathbf{x}_{ij}} \right)^2, \quad (11)$$

where \mathbf{x}_{ij} is the 3-dimensional vector of the coordinates of particle j in slice i , such that $\mathbf{R}_i = (\mathbf{x}_{i1}, \mathbf{x}_{i2}, \dots, \mathbf{x}_{iN})$. This form of the effective action leads to an error of the order of $P(\beta/P)^5$ in the partition function and allows us to significantly reduce the Trotter number required for convergence as compared to the primitive action (see Section V).

The quantum correction to the potential requires the evaluation of the first-principles forces $\mathbf{F}_j = -\partial E_0/\partial \mathbf{x}_j$ in the ground electronic state. The cost of this operation is of the same order of magnitude as the rest of the electronic structure calculation, at least in most *ab initio* or density functional schemes. In contrast, second and higher-order derivatives are sufficiently expensive to evaluate that the computational advantages of a more accurate short-time action are lost.

2. Normal modes sampling

The above expression for the partition function can be directly used to set up a Metropolis MC simulation scheme by assigning the appropriate Boltzmann weight to each configuration of the $N \times P$ -dimensional isomorphic classical system. However, as quantum effects increase, the degree of discretisation must be increased to maintain accuracy. Since the harmonic force constant between adjacent beads on the quantum polymer is $mP/\beta\hbar^2$, increasing the Trotter index results in increasingly stiff harmonic links and the computational problem of ensuring the ergodicity of the Metropolis walk becomes intractable. An intuitively appealing and computationally simple way for circumventing this difficulty comes from considering the normal modes of the quantum polymer²⁴. In the absence of an interaction potential, all Cartesian degrees of freedom of the system are decoupled. For a single degree of freedom the harmonic intra-polymer potential is given by $V_p = (mP/2\beta\hbar^2) \sum_{l=1}^P (x_l - x_{l+1})^2$. Diagonalization of the second derivative matrix of this potential leads to the normal coordinates, $\{Q_k\}, k = 1, \dots, P$,

$$Q_k = (1/\sqrt{P}) \sum_{l=1}^P x_l \exp(2\pi ikl/P). \quad (12)$$

In the normal mode representation, the kinetic energy contribution to the path action is

$$\int_0^{\beta\hbar} \frac{m}{2} \left(\frac{dx}{du} \right)^2 du = \frac{2mP}{\beta\hbar^2} \sum_{k=1}^P |Q_k|^2 \sin^2(\pi k/P). \quad (13)$$

The zero-frequency mode ($k = P$) corresponds to motion of the center-of-mass of the polymer and makes no contribution to the kinetic energy. All other normal modes would be Gaussian distributed with variance $\sigma_k^2 = \beta\hbar^2/4mP \sin^2(\pi k/P)$ if they corresponded to free particles. The potential energy term couples these normal modes and cause distortions from the free-particle distribution. The low-frequency modes correspond to large, collective motions of all beads of the polymer, while the high-frequency modes cause small, local path fluctuations. The normal modes are then used as Metropolis variables and the displacements scaled according to the Gaussian dispersions associated with each normal mode.

The canonical ensemble average of an observable O is given by

$$\langle O \rangle = Tr\{\hat{\rho}\hat{O}\}/Tr\{\hat{\rho}\}, \quad (14)$$

where \hat{O} is the corresponding quantum mechanical operator. If the operator \hat{O} is diagonal in the coordinate representation, then

$$\langle O \rangle = \int d\mathbf{R} O(\mathbf{R}) \rho(\mathbf{R}, \mathbf{R}; \beta). \quad (15)$$

Our MC strategy samples configurations \mathbf{R} with probability proportional to $\rho(\mathbf{R}, \mathbf{R}; \beta)$, such that equilibrium averages can be readily estimated via discrete summations. Dynamical variables that can be related to the partition function are also straightforward to obtain using thermodynamic estimators. With our choice of the short-time action, thermodynamic estimators of the total energy $\langle E \rangle$, the kinetic energy $\langle K \rangle$ and the potential energy $\langle V \rangle$ are given by

$$\langle V \rangle = \langle U_2 \rangle + 2\langle U_c \rangle \quad (16)$$

$$\langle K \rangle = \langle U_1 \rangle + \langle U_c \rangle \quad (17)$$

$$\langle E \rangle = \langle U_1 \rangle + \langle U_2 \rangle + 3\langle U_c \rangle, \quad (18)$$

where

$$U_1 = \frac{3NP}{2\beta} - \sum_{i=1}^P \frac{mP(\mathbf{R}_i - \mathbf{R}_{i+1})^2}{2\beta^2\hbar^2} \quad (19)$$

$$U_2 = \frac{1}{P} \sum_{i=1}^P E_0(\mathbf{R}_i) \quad (20)$$

$$U_c = \frac{1}{P} \frac{\beta^2\hbar^2}{24mP^2} \sum_{i=1}^P \sum_{j=1}^N \left(\frac{\partial E_0(\mathbf{R}_i)}{\partial \mathbf{x}_{ij}} \right)^2. \quad (21)$$

B. Electronic structure calculations

The calculation of the electronic energies is carried out within the framework of DFT. For a given nuclear configuration, Kohn-Sham single-particle equations²⁵ are solved self-consistently for the electronic density, and the total energy and forces are computed accordingly. Kohn-Sham orbitals are expanded in a Gaussian basis set.

The electronic density is also expanded in an additional Gaussian basis set²⁶. The coefficients for the fit of the electronic density are computed by minimizing the error in the Coulomb repulsion energy. The use of this procedure results in an important speedup, since the cost

of evaluating matrix elements reduces from $O(N^4)$ to $O(N^2M)$ (N is the number of functions in the orbital set, and M the number of functions in the auxiliary set, typically of size comparable to N).

Matrix elements of the exchange-correlation potential are calculated by a numerical integration scheme based on grids and quadratures proposed by Becke²⁷. During the self-consistency cycle, the integration is performed on a set of coarse atom-centered, spherical grids. At the end of the self-consistent procedure, the exchange-correlation energy is evaluated using an augmented, finer grid. This strategy of combining coarse and fine grids results in a considerable gain in computational efficiency, which is very important because this part is one of the main bottlenecks of the calculation.

The exchange-correlation term is described a gradient corrected NLDF level. Correlation is given by the parameterization of the homogeneous electron gas of Vosko et al.²⁸ supplemented with the gradient corrections proposed by Perdew²⁹. Gradient corrections to the exchange term are taken from Becke³⁰.

The first derivatives of the energy with respect to the nuclear coordinates, required by the fourth-order effective action, are evaluated by taking analytical derivatives of one-electron and Coulomb terms, while the exchange-correlation contribution is obtained by numerical integration⁵.

IV. GROUND STATE PROPERTIES OF CLASSICAL Li_4 AND Li_5^+

A. Validation of the basis set and optimized geometries

We have analyzed five different basis sets for Li_4 and Li_5^+ . The first one (labeled 1) is the standard 3-21G basis³¹. The second set (labeled 2) is a double zeta plus polarization basis set, optimized for DFT calculations³². The third one (labeled 3) is the standard 6-311G basis³³, the fourth set (labeled 4) is the 6-311G set augmented with a polarization function (6-311G*), and finally the fifth set (labeled 5), consists of a large uncontracted basis set (13s/9p/1d), proposed by Dunning³⁴. The calculations performed with basis sets optimized for standard ab-initio calculations (labeled 1, 3, 4, and 5) have been carried out using an uncontracted auxiliary basis set with a scheme (7s/3p/3d), as proposed in Ref. 32 and 10. The calculations performed with basis set 2 have been carried out using an auxiliary basis set proposed in Ref. 32, with a scheme (7s/2p/1d). Full geometry optimizations without symmetry constraints have been performed in all cases.

In agreement with previous work^{10,15}, only one stable minimum with a rhombus geometry has been found for Li_4 (see Fig. 2), while for Li_5^+ we found four stable local minima (also shown in Fig. 2). The highest energy

isomer, i.e. isomer I, consists of two triangles which lie on the same plane, joined by a shared central atom. The second isomer, i.e. isomer II, is similar to isomer I, but now the triangles lie on perpendicular planes. The third isomer, i.e. isomer III, has C_2 symmetry, and can be described as an isosceles triangle plus a dimer. The dimer is located perpendicularly to the plane of the triangle, close to its shortest side. The fourth isomer, i.e. isomer IV, has a trigonal bipyramidal structure. It should be pointed out that neither isomer II nor isomer III have been reported in earlier works, probably because of symmetry constraints used during the geometry optimization procedure. The basis set dependence of the binding energies is shown in Figure 3. Relevant structural parameters for all basis sets considered here are given in Table I. Our results for basis set 4 agree with those reported for the same functional and basis set in Ref. 15 for Li_4 and for isomers I and IV of Li_5^+ .

The data in Figure 3 and Table I show that calculations performed using basis set 2 yielded results that deviate considerably from the ones obtained using the very large basis set 5, which can be considered as almost converged. Even if the errors in computed bond lengths and binding energies are not too large (about 5 % for bond lengths and 5-10 % for binding energies), calculations carried out using basis set 2 fail in reproducing the energy sequence of isomers of Li_5^+ . This can be ascribed to the fact that the description of the p -shell using this set is rather poor, since it contains only one function. On the other hand, calculations performed with basis sets 1, 3 and 4 yield the same energy ordering for isomers of Li_5^+ and structural results within 2-3% from the almost converged, basis set 5, values.

Basis set superposition error (BSSE)³⁵ calculations for Li_4 yield 14.36, 1.00, 0.96, 2.34, and 0.13 kJ/mol, for basis sets 1, 2, 3, 4, and 5, respectively. It is clear that in order to reduce BSSE, and obtain meaningful interaction energies, a better description of the p -shell than the one provided by the small basis set 1 is required.

TABLE I. Selected geometrical parameters of Li_4 and Li_5^+ (in \AA). Atoms are labeled as in Figure 2.

System		Set 1	Set 2	Set 3	Set 4	Set 5	
Li_4	d_{12}	2.658	2.678	2.638	2.625	2.622	
	d_{13}	3.068	3.117	3.050	3.042	3.039	
Li_5^+	d_{23}	2.879	2.889	2.853	2.853	2.853	
isomer I	d_{12}	3.114	3.144	3.105	3.105	3.104	
Li_5^+	d_{23}	2.888	2.905	2.868	2.860	2.854	
	isomer II	d_{12}	3.099	3.155	3.101	3.090	3.095
Li_5^+	d_{14}	2.713	2.735	2.695	2.680	2.672	
	isomer III	d_{23}	2.851	2.857	2.842	2.823	2.825
		d_{15}	3.035	3.053	3.012	3.012	3.004
	d_{34}	3.353	3.485	3.360	3.345	3.352	
Li_5^+	d_{12}	2.772	2.800	2.754	2.734	2.729	
	isomer IV	d_{14}	3.207	3.250	3.196	3.186	3.184

In view of these results, the intermediate basis set 3 (6-311G), which yields results close to the ones obtained with the larger sets is chosen to perform the electronic structure calculations required in the MC simulations. The relative energies with respect to the most stable isomer, isomer IV, for isomers I, II, and III, are 17.58, 15.16, and 9.67 kJ/mol, respectively, for calculations using basis set 3, compared with 19.38, 17.08, and 11.01 kJ/mol, respectively, using the large set 5.

B. Electronic properties: dipole moments, Mulliken population charges and eigenvalues

The Li_4 cluster is non-polar (vanishing dipole moment) for symmetry reasons. Li_5^+ is a charged system, so its dipole moment depends on the choice of the origin. However, it is customary to evaluate the dipole moment using the center of charge as the origin, and in that case it provides a useful indicator of the asymmetry of the charge distribution, and could also be experimentally relevant. Isomers I, and II are non polar, isomer IV is only slightly polar, but isomer III is considerably polar. The dipole moments of isomers III and IV, computed using basis set 3, are 1.163 D and 0.017 D , respectively. Mulliken population charges³⁶ are also useful indicators of the charge distribution. Results obtained with basis set 3 for Li_4 and the four isomers of Li_5^+ are shown in Table II. Significant differences are observed between different isomers, even between isomers I and II which are very similar both, geometrically and energetically. Both quantities provide useful indicators of isomerization during the MC simulations in the Li_5^+ case.

In addition, we present the two highest occupied and two lowest unoccupied molecular orbital energies for Li_4 and the four isomers of Li_5^+ in Table II. The HOMO-LUMO gap is quite large in all cases, with values around 1 eV. Therefore, it is unlikely that either thermal or quantum fluctuations will contribute to its closure.

TABLE II. Mulliken populations and orbital energies of Li_4 and Li_5^+ computed with basis set 3. (in rA and eV). Atoms are labeled as in Figure 2. The two lowest energy unoccupied and two highest energy occupied orbital energies are given.

	Li_4	Li_5^+ (I)	Li_5^+ (II)	Li_5^+ (III)	Li_5^+ (IV)
q ₁	0.2067	0.5403	0.0419	0.2250	0.3959
q ₂	0.2067	0.1149	0.2395	0.1808	0.3603
q ₃	-0.2067	0.1149	0.2395	0.1808	0.3603
q ₄	-0.2067	0.1149	0.2395	0.2250	-0.0583
q ₅	-	0.1149	0.2395	0.1878	-0.0583
ϵ_{N-1}	-3.9334	-7.2535	-7.2355	-7.8535	-8.1536
ϵ_N	-2.8986	-6.6867	-6.6703	-6.5560	-6.6603
ϵ_{N+1}	-2.0169	-5.3772	-5.0774	-5.4975	-5.7065
ϵ_{N+2}	-1.6806	-5.0904	-5.0774	-5.4562	-5.7002

V. RESULTS OF THE PIMC-DFT SIMULATIONS

A. Sampling strategy and convergence of the path integral with the degree of discretisation

We used a simple Metropolis algorithm for the PIMC simulations with each trial move consisting of an attempt to move all the normal modes associated with all the particles. Two different step-sizes were used: δ_c and δ_s . The maximum displacement of the center-of-mass was set by δ_c , and that of the normal modes of order k – associated with a length scale σ_k – by $\sigma_k \times \delta_s$. We have analyzed the possibility of introducing an additional convergence parameter k^* , such that modes with $k < k^*$ or $k > P - k^*$ are moved with a relatively small step size, $\delta_s \times \sigma_k$, while those associated with small length scale fluctuations are moved by amounts proportional to $\delta_l \times \sigma_k$ ($\delta_l > \delta_s$). However, it turned out that, in this particular case, a single step size δ_s for all values of k was efficient enough. This is often not the case when a large number of Trotter slices is used. The various parameters were adjusted to keep the overall acceptance ratio around 50% though occasional runs were used with acceptance ratios between 40% and 60%. The same displacement parameter for the center-of-mass δ_c was used for both classical and quantum simulations.

Simulations on the Li_2 dimer using a classical potential fitted to first-principles calculations were used to check the convergence of various properties with the degree of discretisation.

Table III gives the PIMC results for the expectation value of the potential and kinetic energies using the primitive action and the fourth-order corrected form of the action. It can be observed that convergence to within the statistical error bars occurs with a Trotter number of just 4 when using the fourth-order correction, in contrast to 16 when using the primitive action. Errors in $\langle V \rangle$ are an order of magnitude less than those in $\langle K \rangle$.

TABLE III. Convergence data for Li_2 at 100 K . Number of MC configurations is 5.12 million with acceptance ratios between 0.4 and 0.7. Error bars are given in brackets. First two columns correspond to results using the primitive approximation and the last two to results obtained using the fourth order correction to the effective action. Energies are expressed in K .

m	$\langle V \rangle$	$\langle K \rangle$	$\langle V \rangle$	$\langle K \rangle$
1	-9521.78 (0.12)	300.0 (0.0)	-9485.82 (0.14)	335.7 (0.1)
2	-9491.74 (0.15)	330.3 (0.5)	-9454.41 (0.15)	366.2 (0.7)
4	-9465.76 (0.26)	355.4 (1.0)	-9446.69 (0.31)	372.8 (0.9)
8	-9453.39 (0.45)	366.5 (1.5)	-9447.10 (0.32)	371.8 (2.4)
16	-9449.79 (0.40)	373.2 (7.6)	-9447.50 (0.44)	371.1 (7.0)

This is typical of the relatively facile convergence of expectation values of operators diagonal in the coordinates as opposed to those than must be evaluated using thermodynamic estimators. In our experience, structural quantities such as pair distribution functions converge even faster than the potential energy. The increase in the error bars – at constant number of MC configurations – as the Trotter number is increased is also typical of PIMC simulations. Based on our tests with Li_2 we used a Trotter number of 4 at 100K and 8 at 50K for the larger clusters.

We have performed a series of classical and quantum Monte Carlo simulations for Li_4 and Li_5^+ clusters, with temperatures ranging from 50 K to 200 K . Each of them consisted of 10000-15000 Monte Carlo steps, preceded by around 1000 steps of thermalization. We stored atomic coordinates, energies, eigenvalues, Mulliken population charges and dipole moment for each MC step, for later analysis.

In the following we will concentrate only in structural parameters, one-electron eigenvalues, and dipole moments, leaving aside other thermodynamical properties which would need longer simulations to reduce the statistical error bars to useful values.

B. Results for Li_4 and Li_5^+

As mentioned in Section IV, Li_4 has a single, deep minimum at the 1A singlet state, in the form of a planar rhombus. Due to this fact the cluster is very rigid and thermal and/or quantum effects basically sample the PES around the minimum. The Li_5^+ cluster constitutes a somewhat richer example due to the existence of several isomers. In particular, it is interesting to analyze the possibility of thermal activation and quantum tunneling between different regions of configuration space. In order to explore different regions of the PES, classical simulations were started from three different isomers, namely the ground state (isomer IV), and two higher energy configurations (isomers I and III). After a few thousand MC steps it was observed that the second and third simulations were attracted towards the ground state basin, showing that our MC strategy is quite effective in equilibrating and exploring configuration space, possibly because interconversion barriers were low. Based on this, quantum simulations were started from the ground state (isomer IV) and, in order to facilitate the detection of possible tunneling behavior, also from the first excited isomer (isomer III). Again, the isomerization towards the ground state was observed in this latter; the polymer moved as a whole, without showing any signature of tunneling. Let us mention that none of the higher-energy isomers appeared again during the simulation, although structures slightly reminiscent of isomer III (the closest in energy to the ground state) were observed. In other words, Li_5^+ appears to be unable to sample metastable re-

gions of configurational space out from the ground state.

Figure 4(a) shows the radial distribution function $g(r)$ of Li_4 in the classical case, and for different temperatures. It can be observed that the peaks are approximately centered at the optimized zero-temperature distances. Temperature effects consist basically of broadening the peaks; the first of them, corresponding to the first neighbour shell, almost disappears above 200 K . In Figure 4(b) we show the effects of the quantum nature of the nuclei by comparing simulations performed at 50 K using the classical and quantum schemes. It can be observed that quantum effects generate a pronounced broadening of the peaks, thus demonstrating the importance of their inclusion.

In Figure 5 we show the radial distribution functions $g(r)$ for Li_5^+ in the classical (a) and quantum (b) cases. The main panels contain the distribution averaged over all the 5 particles. Two groups of atoms can be identified: a first one composed of three atoms more strongly bound, which form the central triangle of the bipyramidal structure IV, and a second one composed by the two external atoms. The upper inset shows the partial $g(r)$ corresponding to these two groups in the classical case at 100 K , and the lower inset in the quantum case at 50 K . No qualitative difference with Li_4 can be observed.

The trends discussed above also hold for the electronic properties, i.e. the distribution of one-particle eigenvalues. As can be observed in Figure 6(a), the HOMO and LUMO eigenvalue distributions for Li_5^+ exhibit significant broadenings upon temperature increase. It is to be remarked that the widths are different for different eigenvalues, a fact that could be reflected in the temperature dependence of the optical photoabsorption spectrum³⁷. Similar broadenings can be observed in the lower panel, corresponding to the quantum and classical simulations for Li_5^+ performed at 50 K . As advanced above, the minimum HOMO-LUMO distance never becomes smaller than about 0.5 eV, so that quantum effects cannot promote an eigenvalue crossing which would result in a major modification of the electronic properties.

Another important quantity is the electric dipole moment, because of its experimental relevance. For Li_4 the dipole moment vanishes at zero temperature due to symmetry considerations. However, at finite temperature the cluster samples regions of the PES characterized by a finite dipole moment, such that the mean value is non-vanishing. A more pronounced effect of the same type can be observed in the quantum simulations. The averages computed using the classical and quantum schemes at 50 K are (0.17 ± 0.07) and (0.29 ± 0.15) D, for Li_4 and (0.14 ± 0.07) and (0.25 ± 0.12) D for Li_5^+ , respectively. The quantum dipole moment averages and distributions obtained at 50 K are similar to those obtained classically at about 100 K .

It is interesting to note that where structural properties are concerned, the overall effect of considering quantum nuclei is qualitatively similar to the effect of increasing temperature in the classical simulations. For

the closed-shell Li clusters considered in this work the classical temperature equivalent to the quantum system at 50 K is around 150 K . However, the dipole moment and eigenvalue distributions obtained using the quantum mechanical scheme at 50 K are qualitatively similar to those obtained within the classical scheme at about 100 K . This points out an important difference between the two types of correlations involved in the statistical mechanics of quantum systems, namely coherent quantum fluctuations as opposed to incoherent thermal fluctuations. These appear to behave in different ways according to the physical properties under consideration.

Further characterization of the wave packet behaviour of the nuclei is provided by the imaginary-time correlation function, $R^2(t - t') = \langle |r(t) - r(t')|^2 \rangle$, where $0 < \tau = t - t' < \beta\hbar$. The value at $\tau = \beta\hbar/2$ is particularly important because it gives an estimation of the quantum delocalization of the nuclei. The delocalization length, or gyration radius, is about 0.15 \AA for both Li_4 and Li_5^+ at 50 K . The imaginary time correlation function for Li_4 is shown in Figure 7, averaged for atoms 1 and 2 (lower curve), and for 3 and 4 (upper curve). It can be noticed that the two atoms which are more strongly bound (1 and 2 in Figure 2) are less delocalized than the other two, as may be expected.

VI. CONCLUSIONS AND OUTLOOK

We have introduced a novel method for simulating the statistical mechanics of quantum nuclei interacting through first-principles potentials, i.e. that derive directly from the electronic structure. The scheme presented and discussed here combines a path integral description of the nuclear variables with an adiabatic, ground state, density functional description of the electronic degrees of freedom. In the present scheme we have chosen a specific (NLDF-Gaussian) formulation to solve the electronic structure problem, but it is important to stress that any other implementation is perfectly valid and compatible with the present scheme, e.g. *ab initio* quantum chemical approaches like Hartree-Fock or MP2, and/or different localized (LCAO, LMTO) or extended (pseudopotential or augmented PW) basis sets. Moreover, the present scheme is extremely simple to interface with any electronic structure code, since the only input needed to compute the statistical weights are the (self-consistently) converged energy and forces. MD sampling schemes are more involved in this respect.

We have shown the adequacy and the performance of this methodology by simulating quantum nuclear effects in the clusters Li_4 and Li_5^+ . The number of imaginary-time slices needed to achieve convergence to a relative error of 0.5% in the nuclear kinetic energy is 4 at a temperature of 100 K , and 8 at 50 K . The same level of accuracy is obtained only with 16 slices (at 100 K) if the primitive approximation to the action is used. This rep-

resents a gain of a factor of 4, which is very important due to the high computational cost of these simulations. The level of gain depends, however, on the shape of the potential energy surface sampled by the nuclei.

The results presented here for the above clusters show that, at temperatures below 50 K , quantum nuclear effects are crucial to account for their structural and electronic properties. Pair correlation functions are quite broadened with respect to the classical counterparts, to a level that similar distributions would be obtained for an effective temperature of about 150 K if only thermal, and not also quantum, fluctuations were considered. The results at $T = 50$ K can be considered to be representative of the ground state, as quantum nuclear effects largely overcome thermal motion. Electronic properties like one-electron eigenvalues and dipole moments show the same type of broadened distributions, although the effective classical temperature appears to be slightly lower, around 100 K , instead of 150 K . This is to emphasize that quantum effects cannot be readily mimicked by adding extra thermal fluctuations, because the correlations involved are of a completely different character: quantum motion is coherent while thermal motion is incoherent.

The simulation technology presented here opens up the possibility of studying the role of light nuclei, especially protons, in biological and chemical systems. The advantage of describing the electronic component using a localized basis set (as Gaussians), as opposed to a PW basis set, for isolated clusters and molecules as well as for gas-phase reactions, is obvious because the vacuum around is easily taken into account. In addition, very often reactive condensed-phase systems and large biological molecules do not need a full quantum description because the relevant chemical processes occur in a circumscribed region of space. For example, enzymatic reactions require a first-principles electronic description only in the vicinity of the active site, while the rest of the system can be treated by means of classical force fields. Therefore, hybrid schemes that combine quantum and classical mechanical descriptions in different spatial regions³⁸ are appropriate for these situations and, in conjunction with the present methodology, constitute a general computational approach appropriate for studying the effects of nuclear delocalization in the above situations. In fact, an insight into the problem of quantum hydrogen-bonding in water has already appeared in the literature³⁹, thus signalling the time for a new and exciting area of multidisciplinary research.

Acknowledgements C. C. would like to thank the Department of Science and Technology, New Delhi for financial support (Grant No. SP/S1/H-36/94). D. A. E. thanks Fundación Antorchas and Universidad de Buenos Aires for financial support, and ICTP for hospitality. R. O. W. thanks Saverio Moroni for helping with the parallelization of the code, and J. K. thanks Dominik Marx for

making accessible his results prior to publication and for helpful discussions. Useful discussions with Erio Tosatti and Pietro Ballone are also acknowledged. The ab initio path integral simulations have been performed in the IBM SP2 parallel machine at SISSA-Trieste.

* Corresponding author. E-mail address: kohanoff@ictp.trieste.it

- ¹ *Clusters of atoms and molecules*, vol. I, Springer Series in Chemical Physics 52, Ed. H. Haberland (Springer, Berlin, 1995).
- ² The experimental situation of alkali metal clusters (including Lithium) is reviewed by: C. Bréchnac in Ref. [1], pp. 255-286. The corresponding theoretical calculations are presented by: V. Bonačić-Koutecký, P. Fantucci, and J. Koutecký, *ibid.*, pp. 37-46.
- ³ R. P. Feynman and A. R. Hibbs, *Quantum Mechanics and Path Integrals* (McGraw-Hill, New York, 1965); R. P. Feynman, *Statistical Mechanics: A Set of Lectures* (Benjamin, Reading, 1976); D. Chandler and K. Leung, *Annu. Rev. Phys. Chem.* **45**, 557 (1994).
- ⁴ For a comprehensive review of density functional methods see, e.g.: R. G. Parr and W. Yang, *Density Functional Theory of Atoms and Molecules* (Oxford University Press, 1989)
- ⁵ D. A. Estrin, G. Corongiu, and E. Clementi, in: METECC, *Methods and Techniques in Computational Chemistry*, ed. E. Clementi (Stef, Cagliari, 1993), Chapter 12.
- ⁶ D. Marx and M. Parrinello, *Z. Phys. B* **95**, 143 (1994); D. Marx and M. Parrinello, *J. Chem. Phys.* **104**, 4077 (1996).
- ⁷ H.-P. Cheng, R. N. Barnett, and U. Landman, *Chem. Phys. Lett.* **237**, 161 (1995).
- ⁸ M. Tuckerman, D. Marx, M. L. Klein, and M. Parrinello, *J. Chem. Phys.* **104**, 5579 (1996).
- ⁹ For recent reviews of computational aspects of path integral simulations see, D. M. Ceperley, *Rev. Mod. Phys.* **67**, 279 (1995); C. Chakravarty, *Int. Rev. Phys. Chem.* (in press).
- ¹⁰ I. Boustani, W. Pewestorf, P. Fantucci, V. Bonačić-Koutecký, and J. Koutecký, *Phys. Rev. B* **35**, 9437 (1987).
- ¹¹ J. Jellinek, V. Bonačić-Koutecký, P. Fantucci, and M. Wiechert, *J. Chem. Phys.* **101**, 10092 (1994).
- ¹² D. Reichardt, V. Bonačić-Koutecký, P. Fantucci, and J. Jellinek, *Z. Phys. D* **40**, 486 (1997).
- ¹³ P. Fantucci, V. Bonačić-Koutecký, J. Jellinek, M. Wiechert, R. J. Harrison, and M. F. Guest, *Chem. Phys. Lett.* **250**, 47 (1996).
- ¹⁴ R. O. Jones, A. I. Lichtenstein, and J. Hutter, *J. Chem. Phys.* **106**, 4566 (1997).
- ¹⁵ R. Rousseau and D. Marx, *Phys. Rev. A* **56**, 617 (1997).
- ¹⁶ C. A. Mead and D. G. Truhlar, *J. Chem. Phys.* **70**, 2284 (1979); M. V. Berry, *Proc. R. Soc. London, Ser. A* **392**, 45 (1984); Y.-S. Wu and A. Kuppermann, *Chem. Phys. Lett.* **201**, 178 (1993).
- ¹⁷ P. Dugourd, J. Chevaleyre, M. Broyer, J. P. Wolf, and L. Wöste, *Chem. Phys. Lett.* **175**, 555 (1990). See also T. C. Thompson, G. Izmirlian Jr., S. J. Lemon, D. G. Truhlar, and C. A. Mead, *J. Chem. Phys.* **82**, 5597 (1985).
- ¹⁸ J. A. Howard, H. A. Joly, R. Jones, P. P. Edwards, R. J. Singer, and D. E. Logan, *Chem. Phys. Lett.* **204**, 128 (1993).
- ¹⁹ P. Ballone and P. Milani, *Phys. Rev. B* **45**, 11222 (1992).
- ²⁰ R. Rousseau and D. Marx, *Phys. Rev. Lett.* (in press).
- ²¹ D. M. Ceperley and E. L. Pollock, *Phys. Rev. Lett.* **56**, 351 (1986); E. L. Pollock and D. M. Ceperley, *Phys. Rev. B* **36**, 8343 (1987).
- ²² C. Pierleoni, D. M. Ceperley, B. Bernu and W. R. Magro, *Phys. Rev. Lett.* **73**, 2145 (1994).
- ²³ M. Takahashi and M. Imada, *J. Phys. Soc. Jpn.* **53**, 3765 (1984).
- ²⁴ K. Runge and G. V. Chester, *Phys. Rev. B* **38**, 135 (1988); J. Cao and B. J. Berne, *J. Chem. Phys.* **99**, 2902 (1993).
- ²⁵ W. Kohn and L. J. Sham *Phys. Rev. A* **140**, 1133 (1965).
- ²⁶ B. I. Dunlap, J. W. D. Connolly, and J. R. Sabin, *J. Chem. Phys.* **71**, 3396, 4993 (1979).
- ²⁷ A. D. Becke, *J. Chem. Phys.* **88**, 1053 (1988).
- ²⁸ S. H. Vosko, L. Wilk, and M. Nusair, *Can. J. Phys.* **58**, 1200 (1980).
- ²⁹ J. P. Perdew, *Phys. Rev. B*, **33**, 8822 (1986); Erratum, *Ibid.*, **34**, 7406 (1986).
- ³⁰ A. D. Becke, *Phys. Rev. A*, **38**, 3098 (1988).
- ³¹ J. S. Binkley, J. A. Pople, and W. H. Wehre, *J. Am. Chem. Soc.* **102**, 939, (1980).
- ³² N. Godbout, D. R. Salahub, J. Andzelm, and E. Wimmer, *Can. J. Chem.* **70**, 560 (1992).
- ³³ R. Krishnan, J. S. Binkley, R. Seeger, and J. A. Pople, *J. Chem. Phys.* **72**, 650 (1980).
- ³⁴ S. Huzinaga, J. Andzelm, M. Klobukowski, E. Radzio-Andzelm, Y. Sakai and H. Tatewaki, Eds, *Gaussian Basis Sets for Molecular Calculations* (Elsevier, Amsterdam, 1984).
- ³⁵ S. F. Boys, and F. Bernardi, *Mol. Phys.* **19** 553, (1970).
- ³⁶ A. Szabo and N. S. Ostlund, *Modern Quantum Chemistry* (Mc-Graw Hill, New York, 1989).
- ³⁷ A. Rubio, J. A. Alonso, X. Blase, L. C. Balbás, and S. G. Louie, *Phys. Rev. Lett.* **77**, 247 (1996).
- ³⁸ D. A. Estrin, J. Kohanoff, D. H. Laría, and R. O. Weht, *Chem. Phys. Lett.* **280**, 280 (1997).
- ³⁹ M. E. Tuckerman, D. Marx, M. L. Klein, and M. Parrinello, *Science* **275**, 817 (1997).

FIG. 1. A schematic representation of a potential energy surface with two minima separated by a barrier. Dashed lines represent different possible values of the zero-point-energy (ZPE): (a) ZPE is larger than the barrier (resonant regime), (b) ZPE is between the bottom of the higher well and the top of the barrier (tunneling regime), (c) ZPE is below the bottom of the higher well (classical regime).

FIG. 2. The single isomer of Li_4 (left panel), and the four isomers of Li_5^+ (right panel). Isomer IV is the most stable, followed by isomer III. Isomers I and II are quite higher in energy, and are almost degenerate.

FIG. 3. Dependence of the energetics of Li clusters on the size of the basis set (BS). BS are ordered in increasing size.

FIG. 4. Pair correlation functions $g(r)$ for Li_4 . The upper panel shows the classical results for temperatures of 50 (solid line), 100 (dashed line), and 200 (dotted-dashed line) K . The lower panel shows the quantum (dashed line) and classical (solid line) results for $T = 50 K$.

FIG. 5. Pair correlation functions $g(r)$ for Li_5^+ . The upper panel shows the classical results for temperatures of 50 (solid line), and 100 (dashed line) K . The lower panel shows the quantum (dashed line) and classical (solid line) results for $T = 50 K$. The insets show the partial $g(r)$ for two groups of atoms, one forming the central triangle and the other consisting of the two external atoms.

FIG. 6. Distribution of HOMO and LUMO one-electron eigenvalues for Li_5^+ . The upper panel shows the classical results for temperatures of 50 (solid line), and 100 (dashed line) K . The lower panel shows the quantum (dashed line) and classical (solid line) results at $T = 50 K$.

FIG. 7. Root-mean-square of the imaginary-time correlation function for Li_4 at 50 K plotted versus k (with $0 \leq k = \beta\hbar/P \leq \beta\hbar$), averaged over atoms 1 and 2 (lower curve), and over atoms 3 and 4 (upper curve). P is the Trotter number, 8 in this case.

Figure 1, Weht, J. Chem. Phys.

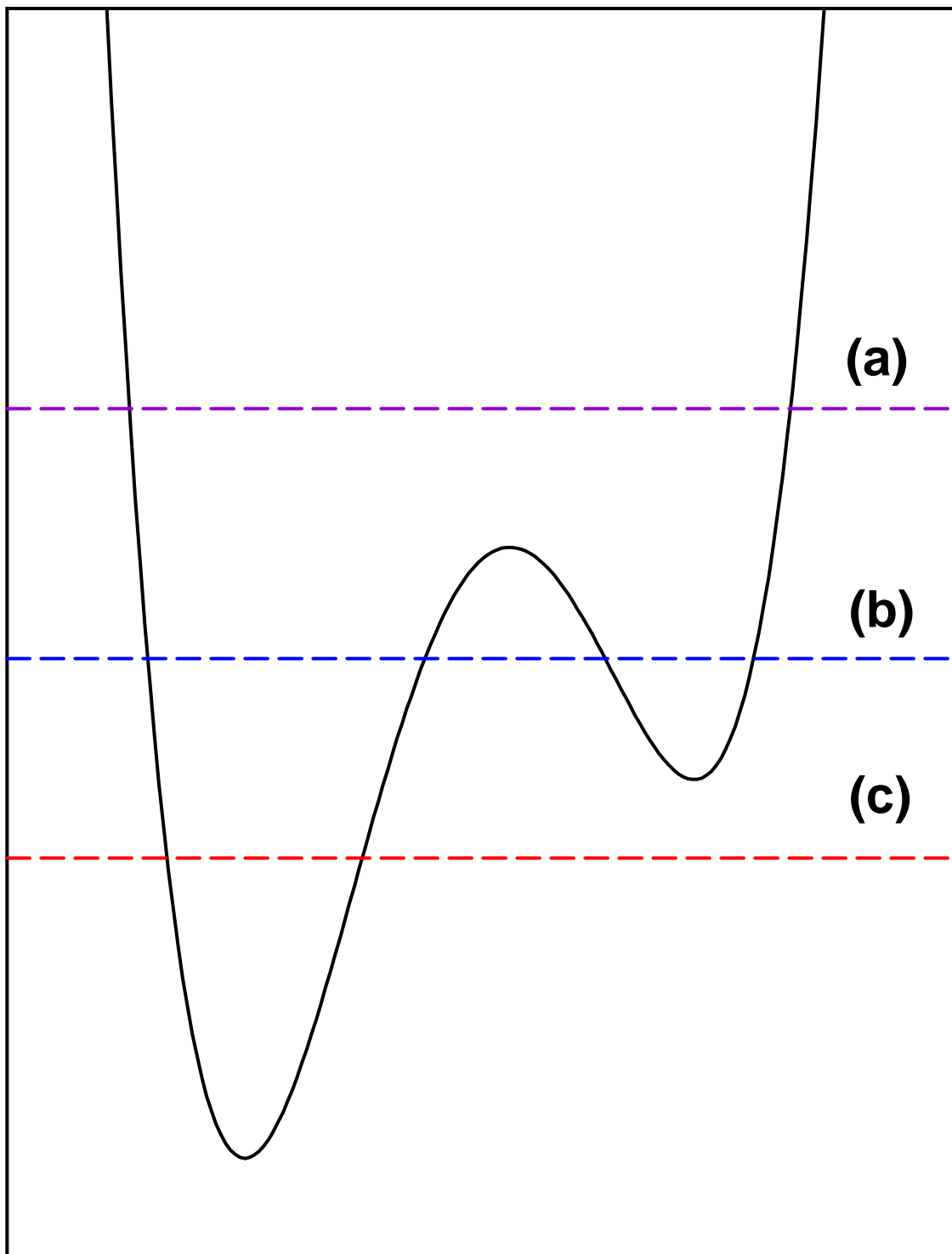


Figure 2, Weht, J. Chem. Phys.

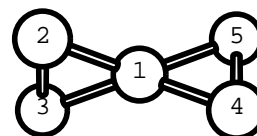
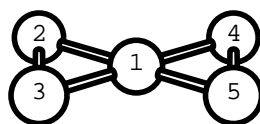
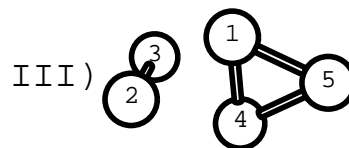
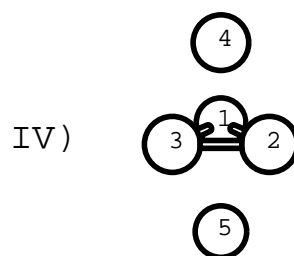
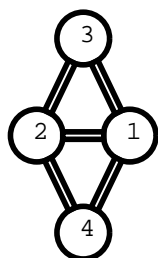


Figure 3, Weht, J. Chem. Phys.

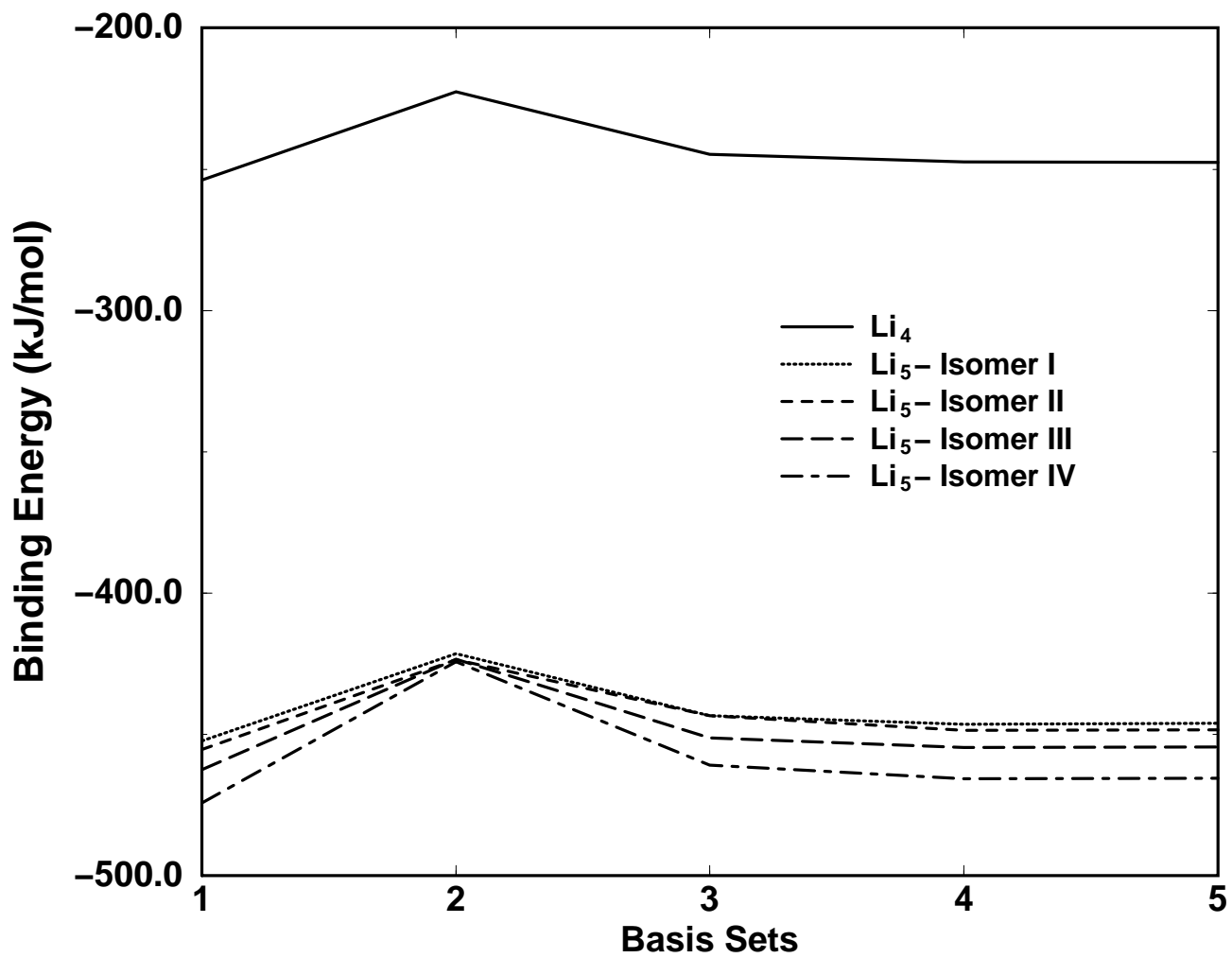


Figure 4, Weht, J. Chem. Phys.

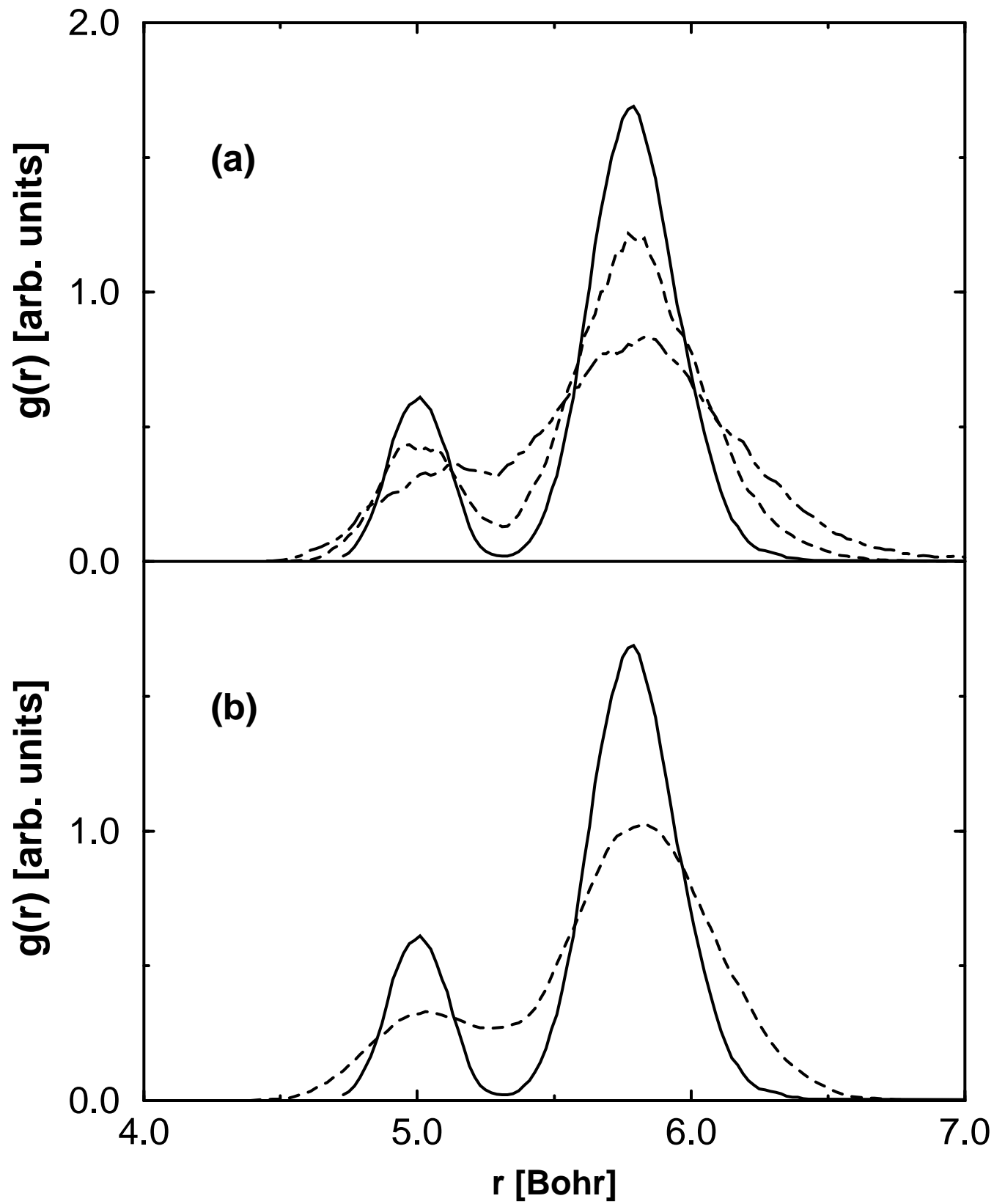


Figure 5, Weht, J. Chem. Phys.

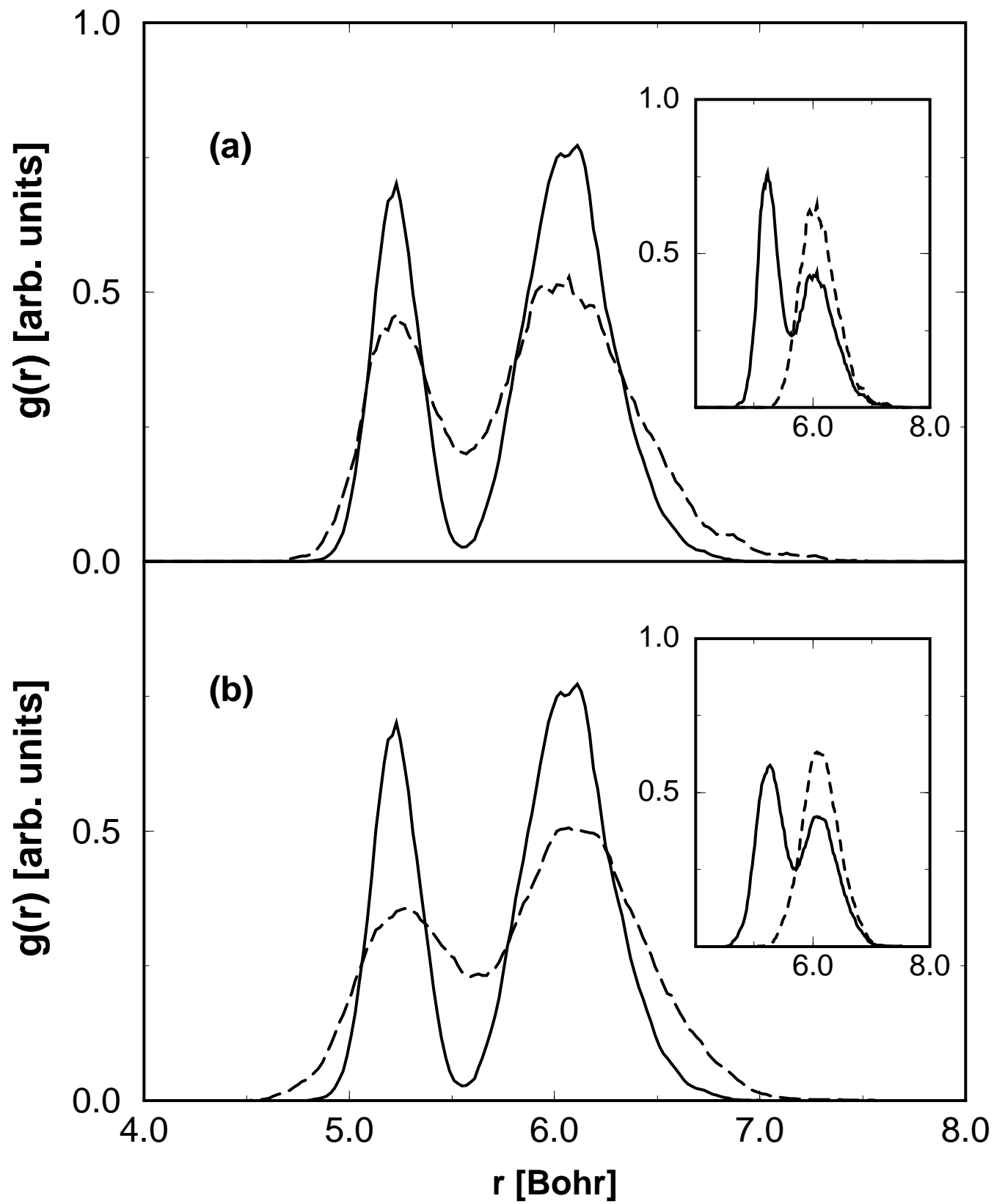


Figure 6, Weht, J. Chem. Phys.

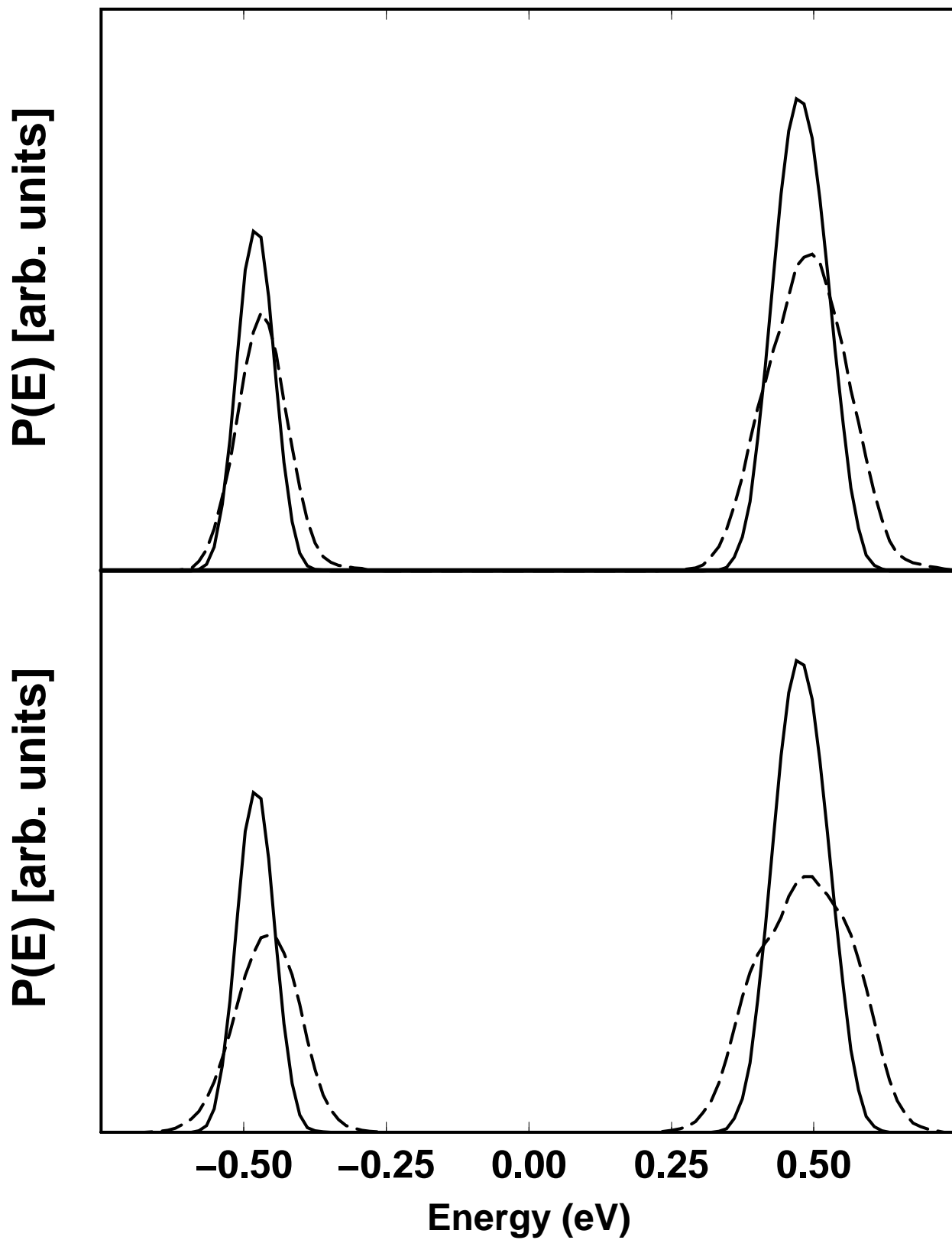


Figure 7, Weht, J. Chem. Phys.

